

**Staircase, Cyclic and Differential Voltammetries of
the 9-Member Square Scheme at Microelectrodes of Any Geometry
with Arbitrary Chemical Stabilization of the Three Redox States**

Ángela Molina^{*,a}, Eduardo Laborda^a, José María Gómez-Gil^a, Richard G. Compton^b

^a *Departamento de Química Física, Facultad de Química, Regional Campus of International Excellence "Campus Mare Nostrum", Universidad de Murcia, 30100 Murcia, Spain*

^b *Department of Chemistry, Physical and Theoretical Chemistry Laboratory, University of Oxford, South Parks Road, OX1 3QZ, Oxford, United Kingdom*

* Corresponding author:

Tel: +34 868 88 7524

Fax: +34 868 88 4148

Email: amolina@um.es

Abstract

Simple analytical expressions are deduced for the cyclic (staircase) and differential cyclic (staircase) voltammetric responses of the 9-member square scheme at the most widely-used microelectrode geometries: disc, (hemi)spheres, cylinders and bands. The generality of the reaction scheme considered enables us to tackle many different and common electrochemical situations where the oxidized, intermediate and/or reduced species of a two-electron transfer also take part in homogeneous chemical equilibria such as protonations, complexations or ion pairings. The effect of the coupled chemical processes on the voltammograms is analyzed at electrodes of different size and shape under a variety of conditions depending on which redox state is chemically stabilized most significantly. Also, working curves for the determination of the formal potentials and the chemical equilibrium constants are given for macro-, micro- and ultramicro-electrodes in cyclic voltammetry and differential cyclic voltammetry.

Keywords: 9-member square scheme; Microelectrodes; Chemical stabilization; Cyclic voltammetry; Differential cyclic voltammetry

1. Introduction

Analytical solutions are deduced for the staircase (SCV) and cyclic (CV) voltammetries of two-step electrode reactions at electrodes of any size and shape in media where the redox species are stabilised to different extents by reaction equilibria in solution such as complexations [1], protonations [2, 3] and ion associations [4, 5]. This is found in a large number of processes [6] impacting on highly diverse fields such as electrocatalysis [5], biocide and drug development [7], biomedicine (electrochemistry of DNA, metalloproteins, enzymes, neurotransmitters, vitamins, etc.) [8, 9] and nanoscience [10]. The electrochemical response of these systems depends on the stability and reactivity of the different oxidation states in solution. Understanding them is essential for the optimization of energy conversion and molecular electronic devices and the design of new compounds, materials and analytical methods.

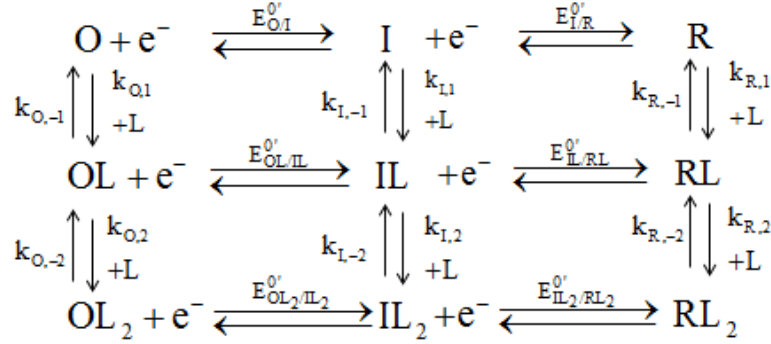
A general analytical theory for single-pulse and cyclic voltammetries of the so-called 9-member square scheme [11, 12] with reversible electron transfers is developed here. Simple explicit solutions are deduced applicable to any electrode geometry, including microelectrodes of different shapes: discs, hemispheres, bands and cylinders. This is of great interest recognising the experimental value of microelectrodes [13] and the complexity of the theoretical modelling of diffusion at certain geometries, most notably the ubiquitously-employed microdiscs. Thus, the theory presented here provides physical insight into the influence of mass transport on these electrochemical systems.

The features of the cyclic voltammograms of the 9-member square mechanism are investigated at electrodes of different geometry under transient and steady state conditions for different values of the formal potentials and for distinctly different chemical stabilisation of the three redox states. Depending on the electrode geometry and the difference between the formal potentials, appropriate procedures based on cyclic voltammetry [14, 15] and differential cyclic voltammetry [16] are established to elucidate the chemistry of the redox species in solution and to determine the corresponding equilibrium constants.

2. Theory

Consider an electrode process that follows a 9-member square mechanism as shown in

Scheme I:



Scheme I. 9-member Square Scheme mechanism assuming all the chemical steps as complexation or dissociation. $E_{\text{OL}_j/\text{IL}_j}^{0'}$ (V) and $E_{\text{IL}_j/\text{RL}_j}^{0'}$ (V) ($j=0,1,2$) are the formal potentials of the redox couples OL_j/IL_j and IL_j/RL_j , respectively. $k_{\text{X},n}$ (s^{-1}) ($\text{X} \equiv \text{O}, \text{I}, \text{R}$, $n=1,2$) is the pseudo-first order association rate constant where the concentration of species L is assumed to be the same at any time and point of the electrolyte solution (see Eq. (9)), and $k_{\text{X},-n}$ (s^{-1}) the first-order dissociation rate constant.

The concentrations of the participating species after applying a potential-controlled perturbation $E(t)$ obey the following diffusion-reaction differential equation system:

$$\hat{\delta} c_{\text{XL}_j} = \Upsilon_{\text{XL}_j} \quad \left\{ \text{X} \equiv \text{O}, \text{I}, \text{R}; \quad j=0,1,2 \right. \quad (1)$$

where $\hat{\delta}$ is the diffusion operator [18, 19] and $\Upsilon_{\text{XL}_j}(q,t)$ corresponds to the sum of kinetic terms of all the homogeneous chemical reactions a given species (XL_j) takes part in, including cross-redox reactions such as disproportionation-comproportionation reactions, which are not shown in Scheme I [20, 21]. Note that species L is not considered in Eq. (1) because its concentration is assumed to be constant (*i.e.*, $c_{\text{L}}(q,t) = c_{\text{L}}^* \forall q,t$) for being buffered (e.g. protons) or in a large excess with respect to the concentration of electroactive species ($c_{\text{L}}^* / c_{\text{OT}}^* > 10$, [17]).

The boundary conditions of the above problem assuming that only the oxidized species are initially present and that the electrode reactions are reversible (*i.e.*, $k^0 q_{\text{G}} / D > 10$ with k^0

being the standard heterogeneous rate constant and q_G given in the caption of Table 1 [19])

are given by:

$$\left. \begin{array}{l} t = 0, q \geq q^S \\ t > 0, q \rightarrow \infty \end{array} \right\} \begin{cases} c_O(q, t) = c_O^*, \quad c_{OL}(q, t) = c_{OL}^*, \quad c_{OL_2}(q, t) = c_{OL_2}^* \\ c_I(q, t) = c_{IL}(q, t) = c_{IL_2}(q, t) = 0 \\ c_R(q, t) = c_{RL}(q, t) = c_{RL_2}(q, t) = 0 \end{cases} \quad (2)$$

$t > 0, q = q^S$:

$$D_{OL_j} \left(\frac{\partial c_{OL_j}(q, t)}{\partial q_N} \right)_{q=q^S} + D_{IL_j} \left(\frac{\partial c_{IL_j}(q, t)}{\partial q_N} \right)_{q=q^S} + D_{RL_j} \left(\frac{\partial c_{RL_j}(q, t)}{\partial q_N} \right)_{q=q^S} = 0 \quad j = 0, 1, 2 \quad (3)$$

$$\left. \begin{array}{l} c_{OL_j}(q^S, t) = c_{IL_j}(q^S, t) e^{\eta_{OL_j/IL_j}} \\ c_{IL_j}(q^S, t) = c_{RL_j}(q^S, t) e^{\eta_{IL_j/RL_j}} \end{array} \right\} j = 0, 1, 2 \quad (4)$$

where η_{OL_j/IL_j} and η_{IL_j/RL_j} are defined as:

$$\left. \begin{array}{l} \eta_{OL_j/IL_j} = \frac{F}{RT} (E - E_{OL_j/IL_j}^{0'}) \\ \eta_{IL_j/RL_j} = \frac{F}{RT} (E - E_{IL_j/RL_j}^{0'}) \end{array} \right\} j = 0, 1, 2 \quad (5)$$

q_N is the coordinate normal to the electrode surface, q^S is the value of the coordinates at the surface of the electrode and F , R and T have their usual meanings.

Next, we assume that the chemical kinetics is much faster than the mass transport by diffusion so that total equilibrium conditions hold at any point in solution and time of the experiment such that:

$$\left. \begin{array}{l} K_{O,1} = \frac{k_{O,1}}{k_{O,-1}} = \frac{c_{OL}^{eq}(q, t)}{c_O^{eq}(q, t)} = K_{O,1}^c c_L^* \\ K_{I,1} = \frac{k_{I,1}}{k_{I,-1}} = \frac{c_{IL}^{eq}(q, t)}{c_I^{eq}(q, t)} = K_{I,1}^c c_L^* \\ \vdots \\ K_{R,2} = \frac{k_{R,2}}{k_{R,-2}} = \frac{c_{RL_2}^{eq}(q, t)}{c_{RL}^{eq}(q, t)} = K_{R,2}^c c_L^* \end{array} \right\} \forall q, t \quad (6)$$

where $K_{X,n}$ and $K_{X,n}^c$ are the apparent equilibrium constants and the equilibrium constants based on concentrations, respectively, and c_L^* the concentration of species L. Also, it will be considered that all the *electroactive* species have the same diffusion coefficient ($D_O = D_1 = \dots = D_{RL_2} = D$). These two assumptions are reasonable for a number of frequent chemical processes (including protonations, ion pairings and complexations with small ligands [1–4]) that are generally fast and do not lead to any significant alteration of the molecule size.

Under the above conditions (reversible electron transfers, equal diffusion coefficients of the electroactive species and homogeneous chemical reactions at equilibrium conditions), it is convenient to define the total concentration of the pseudo-species XT (\equiv OT, IT, RT):

$$\left. \begin{aligned} c_{OT}(q,t) &= c_O(q,t) + \sum_{j=1}^{n=2} c_{OL_j}(q,t) \\ c_{IT}(q,t) &= c_I(q,t) + \sum_{j=1}^{n=2} c_{IL_j}(q,t) \\ c_{RT}(q,t) &= c_R(q,t) + \sum_{j=1}^{n=2} c_{RL_j}(q,t) \end{aligned} \right\} \quad (7)$$

The differential equation system (1) becomes:

$$\left. \begin{aligned} \hat{\delta}c_{OT}(q,t) &= 0 \\ \hat{\delta}c_{IT}(q,t) &= 0 \\ \hat{\delta}c_{RT}(q,t) &= 0 \end{aligned} \right\} \quad (8)$$

The boundary conditions become:

$$\left. \begin{aligned} t = 0, q \geq q^S & \left\{ \begin{aligned} c_{OT}(q,t) &= c_{OT}^* = c_O^* + c_{OL}^* + c_{OL_2}^* \\ c_{IT}(q,t) &= c_{RT}(q,t) = 0 \end{aligned} \right. \end{aligned} \right\} \quad (9)$$

$t > 0, q = q^S$:

$$\left(\frac{\partial c_{OT}(q,t)}{\partial q_N} \right)_{q=q^S} + \left(\frac{\partial c_{IT}(q,t)}{\partial q_N} \right)_{q=q^S} + \left(\frac{\partial c_{RT}(q,t)}{\partial q_N} \right)_{q=q^S} = 0 \quad (10)$$

$$\left. \begin{aligned} c_{OT}(q^S,t) &= c_{IT}(q^S,t) e^{\eta_{OT/IT}} \\ c_{IT}(q^S,t) &= c_{RT}(q^S,t) e^{\eta_{IT/RT}} \end{aligned} \right\} \quad (11)$$

$\eta_{OT/IT}$ and $\eta_{IT/RT}$ are defined as:

$$\left. \begin{aligned} \eta_{OT/IT} &= \frac{F}{RT} (E - E_{OT/IT}^{0'}) \\ \eta_{IT/RT} &= \frac{F}{RT} (E - E_{IT/RT}^{0'}) \end{aligned} \right\} \quad (12)$$

$E_{OT/IT}^{0'}$ and $E_{IT/RT}^{0'}$ are the *apparent* formal potentials of the first and second electron transfers given by:

$$\begin{aligned} E_{OT/IT}^{0'} &= E_{O/I}^{0'} - \frac{RT}{F} \ln \left(\frac{1 + \sum_{n=1}^2 \beta_{O,n}}{1 + \sum_{n=1}^2 \beta_{I,n}} \right) \\ E_{IT/RT}^{0'} &= E_{I/R}^{0'} - \frac{RT}{F} \ln \left(\frac{1 + \sum_{n=1}^2 \beta_{I,n}}{1 + \sum_{n=1}^2 \beta_{R,n}} \right) \end{aligned} \quad (13)$$

where $\beta_{X,n}$ correspond to the overall formation equilibrium constant:

$$\beta_{X,n} = \prod_{v=1}^n K_{X,v} = \frac{c_{XL_n}(q,t)}{c_X(q,t)} ; \quad X \equiv O, I, R \quad (14)$$

and K_{XL_n} are the *conditional* formation constant for species XL_n .

It is worth noting that from Eqs. (8)-(10) it is immediately deduced that, under the conditions considered here, the total concentration of all the redox species remains constant over the experiment at any point in solution whatever the electrode geometry [19, 22]:

$$c_T = c_{OT} + c_{IT} + c_{RT} = c_{OT}^* ; \quad \forall q, t \quad (15)$$

which, together with the Nernstian conditions (Eqs. (11)), leads to the following expressions for the surface concentrations of the three redox states:

$$\begin{aligned} c_{OT}^S &= \frac{c_{OT}^* e^{\eta_{OT/IT}} e^{\eta_{IT/RT}}}{1 + e^{\eta_{IT/RT}} + e^{\eta_{OT/IT}} e^{\eta_{IT/RT}}} \\ c_{IT}^S &= \frac{c_{OT}^* e^{\eta_{IT/RT}}}{1 + e^{\eta_{IT/RT}} + e^{\eta_{OT/IT}} e^{\eta_{IT/RT}}} \\ c_{RT}^S &= \frac{c_{OT}^*}{1 + e^{\eta_{IT/RT}} + e^{\eta_{OT/IT}} e^{\eta_{IT/RT}}} \end{aligned} \quad (16)$$

These are independent of time and only dependent on the applied potential.

By defining the following linear combination:

$$W(q,t) = 2c_{OT} + c_{IT} \quad (17)$$

the boundary value problem becomes (see Eqs.(8)-(10),(11)):

$$\delta W(q,t) = 0 \quad (18)$$

$$\left. \begin{array}{l} t \geq 0, q \rightarrow \infty \\ t = 0, q = q^S \end{array} \right\} \rightarrow W(q,t) = W^* = 2c_{OT}^* \quad (19)$$

$$t > 0, q \geq q^S \rightarrow W(q^S,t) = W^S = c_{OT}^* \frac{(2e^{\eta_{OT/IT}} + 1)e^{\eta_{IT/RT}}}{1 + (1 + e^{\eta_{OT/IT}})e^{\eta_{IT/RT}}}$$

and the current response, which is not affected by the presence of cross redox reactions, is given by:

$$I = FAD \left[2 \left(\frac{\partial c_{OT}}{\partial q_N} \right)_{q=q^S} + \left(\frac{\partial c_{IT}}{\partial q_N} \right)_{q=q^S} \right] = FAD \left(\frac{\partial W}{\partial q_N} \right)_{q=q^S} \quad (20)$$

2.1. Single-pulse techniques

For this problem it has been demonstrated [19, 23] that the influence of time and electrode geometry can be separated from that of the applied potential, independently of the shape and size of the electrode considered. Thus, the current in single potential step techniques such as chronoamperometry or normal pulse voltammetry can be expressed as:

$$I^{[1]} = FA_G D f_G(q_G^S, t) [W^* - W^S] \quad (21)$$

This can be re-written in the following normalized form, which is independent of the shape and size of the electrode:

$$I_N^{[1]} = \frac{I^{[1]}}{I_D} = \frac{W^* - W^S}{c_{OT}^*} \quad (22)$$

I_D is the diffusion-controlled limiting current:

$$I_D = FA_G D c_{OT}^* f_G(q_G^S, t) \quad (23)$$

and $f_G(q_G^S, t)$ is a function dependent on time and on the geometry of the electrode (see reference [18, 19]). In the Appendix, the analytical solution for single-pulse techniques of the most common particular mechanisms that can be derived from Scheme I are given.

2.2. Staircase cyclic voltammetry and Cyclic voltammetry

Usually, in multipulse techniques, a sequence of potential steps E_1, E_2, \dots, E_p of the same length τ is applied and the current is measured at a certain time, typically at the end of each pulse. Given that the superposition principle is applicable to the mechanism considered here (Eqs. (16)) [18], the expression for the current of the p -th potential pulse can be written as:

$$I^{(p)} = FA_G D \left(\frac{\partial W^{(p)}(q, t)}{\partial q_N} \right)_{q=q^s} = FA_G D \left\{ \sum_{m=1}^p \left[\left(W^{(m-1),s} - W^{(m),s} \right) f_G(t_{m,p}, q_G^s) \right] \right\} \quad (24)$$

where:

$$W^{(m),s} = c_{OT}^* \frac{2e^{\eta_{OT/IT}^{(m)}} e^{\eta_{IT/RT}^{(m)}} + e^{\eta_{IT/RT}^{(m)}}}{1 + e^{\eta_{IT/RT}^{(m)}} + e^{\eta_{OT/IT}^{(m)}} e^{\eta_{IT/RT}^{(m)}}} \quad m=1, 2, \dots, p \quad (25)$$

$$W^{(0),s} = W^* = 2c_{OT}^*$$

$$\eta_{OT/IT}^{(p)} = \frac{F(E^{(p)} - E_{OT/IT}^{(p)})}{RT} \quad (26)$$

$$\eta_{IT/RT}^{(p)} = \frac{F(E^{(p)} - E_{IT/RT}^{(p)})}{RT}$$

$$t_{m,p} = (p - m + 1) \tau \quad (27)$$

and $f_G(t_{m,p}, q_G)$ is given in reference [18, 19].

From Eq. (24), the response in staircase cyclic voltammetry (SCV) [16] can be calculated, taking into account that the potential perturbation for this technique is given by:

$$\left. \begin{aligned} E_m(t) &= E_{init} - (m-1)\Delta E \text{ for } m=1, 2, \dots, N/2 \\ E_m(t) &= E_{fin} + (m - p/2)\Delta E \text{ for } m=N/2, \dots, N \end{aligned} \right\} \quad (28)$$

where ΔE is the step width potential, m refers to the pulse applied and N to the total number of pulses defined as:

$$N = \frac{2|E_{init} - E_{fin}|}{\Delta E} \quad (29)$$

Note that the perturbation in cyclic voltammetry (CV) corresponds to the limit of the SCV response (Eq. (28)) when the step amplitude ΔE is very small (<0.01 mV [24]). Under such

conditions, the pulsed waveform behaves as a ramp with the applied potential being a continuous function of time:

$$\left. \begin{aligned} E(t) &= E_{\text{init}} - \nu t \text{ for } t \leq t_{\text{inv}} \\ E(t) &= E_{\text{fin}} + \nu t \text{ for } t > t_{\text{inv}} \end{aligned} \right\} \quad (30)$$

where t_{inv} is the time at which the scan direction is inverted and the scan rate is: $\nu = dE/dt$. Then, the value of $t_{m,p}$ (Eq. (31)) can be defined for CV as a function of the scan rate and the applied potential as follows:

$$t_{m,p}^{\text{CV}} = \frac{|E_{p-m+1} - E_{\text{init}}|}{\nu}, \quad m=1, 2, \dots, p \quad (31)$$

such that the equation for the CV current at electrodes of any geometry and size can be rewritten as:

$$\Psi^{(p),\text{CV}} = \frac{I^{(p)}}{FA_G c_{\text{OT}}^* \sqrt{Da}} = \frac{1}{c_{\text{OT}}^*} \left\{ \sum_{m=1}^p \left[\left(W^{(m-1),s} - W^{(m),s} \right) f_G \left(\mathfrak{g}_{m,p}, \xi_G \right) \right] \right\} \quad (32)$$

where:

$$a = \frac{F\nu}{RT} \quad (33)$$

$$\xi_d = \sqrt{\frac{D}{q_G^2} \frac{RT}{F\nu}} \quad (34)$$

$$\mathfrak{g}_{m,p} = \begin{cases} \frac{F}{RT} (E_{p-m+1} - E_{\text{init}}) & m \leq N/2 \\ \frac{F}{RT} (E_{p-m+1} - E_{\text{init}} + 2E_{\text{fin}}) & m > N/2 \end{cases} \quad (35)$$

and $f_G(\mathfrak{g}_{m,p}^{\text{CV}}, \xi_G)$ is given in Table 1 and $(N/2)$ is the number of pulses of each (forward and reverse) scan.

Electrode	$f_G(\vartheta_{m,p}, \xi_G)$	$f_{G,micro}$
Disc (radius r_d , Area $A_d = \pi r_d^2$)	$\frac{4}{\pi} \xi_d \left(0.7854 + \frac{0.44315}{\xi_d \sqrt{\vartheta_{m,p}}} + 0.2146 \exp \left(-\frac{0.39115}{\xi_d \sqrt{\vartheta_{m,p}}} \right) \right),$ <p style="text-align: center;">with $\xi_d = \sqrt{\frac{D}{r_d^2} \frac{RT}{Fv}}$</p>	$\frac{4}{\pi} \xi_d$
Sphere (radius r_s , Area = $4\pi r_s^2$)	$\xi_s + \frac{1}{\sqrt{\pi \vartheta_{m,p}}} \quad \text{with } \xi_s = \sqrt{\frac{D}{r_s^2} \frac{RT}{Fv}}$	ξ_s
Band (height w , length l , Area = wl)	$\xi_b + \frac{1}{\sqrt{\pi \vartheta_{m,p}}} \quad \text{if } (\xi_b^2 \vartheta_{m,p}) < 0.4$ $0.25 \sqrt{\frac{\pi}{\vartheta_{m,p}}} e^{-0.4 \sqrt{\pi \vartheta_{m,p}} \xi_b} + \frac{\pi \xi_b}{\ln(5.2945 + 5.9944 \sqrt{\vartheta_{m,p}} \xi_b)} \quad \text{if } (\xi_b^2 \vartheta_{m,p}) \geq 0.4$ <p style="text-align: center;">with $\xi_b = \sqrt{\frac{D}{w^2} \frac{RT}{Fv}}$</p>	$\frac{2\pi \xi_b}{\ln[64 \xi_b^2 \vartheta_{m,p}]}$
Cylinder (radius r_c , length l , Area = $2\pi r_c l$)	$\frac{1}{\sqrt{\pi \vartheta_{m,p}}} e^{-0.1 \sqrt{\pi \vartheta_{m,p}} \xi_c} + \frac{\xi_c}{\ln(5.2945 + 1.4986 \sqrt{\vartheta_{m,p}} \xi_c)} \quad \text{with } \xi_c = \sqrt{\frac{D}{r_c^2} \frac{RT}{Fv}}$	$\frac{2\xi_c}{\ln[4 \xi_c^2 \vartheta_{m,p}]}$

Table 1. Expressions for the functions $f_G(\vartheta_{m,p}, \xi_G)$ and $f_{G,micro}$ for the most usual electrode geometries considered. Where q_G is given by: $q_G = r_d$ for discs; $q_G = r_s$ for spheres or hemispheres; $q_G = r_c$ for cylinders; $q_G = w$ for bands; $\vartheta_{m,p}$ is given in Eq. (35).

3. Results and Discussion

3.1. Effect of the chemical stabilization of the different redox states

In the absence of coupled chemical processes and/or kinetic constraints, the voltammetric response of two-electron electrode processes is governed by the thermodynamic stability of the intermediate (*i.e.*, the difference between the two formal potentials) [1, 25–30]). Nevertheless, the experimental voltammetric response may differ from the above due to the 'stabilization' of a particular redox state as a result of slow electrode kinetics [31, 32] and/or coupled chemical reactions in solution [1, 29, 33]. The latter 'chemical stabilisation' effects for the case of very fast kinetics can be studied with the analytical expressions reported in Section 2 that enable us to envisage and cover many different particular situations depending on whether one or more redox states undergo a significant chemical stabilisation that affects the value of the corresponding *apparent* formal(s) potential(s) and the magnitude of such effect. According to Eqs. (13), this is quantified by the values of G_O , G_I and G_R defined as:

$$\begin{aligned} G_O &= \beta_{O,1} + \beta_{O,2} \\ G_I &= \beta_{I,1} + \beta_{I,2} \\ G_R &= \beta_{R,1} + \beta_{R,2} \end{aligned} \quad (36)$$

such that the difference between the apparent formal potential that defines the behaviour of the 9-member square scheme can be written as:

$$\Delta E_{app}^{0'} = (E_{1/R}^{0'} - E_{O/I}^{0'}) + \frac{RT}{F} \ln \left\{ \frac{(1+G_O)(1+G_R)}{(1+G_I)^2} \right\} \quad (37)$$

Then, it is clear that $\Delta E_{app}^{0'} < \Delta E^{0'}$ when the stabilization of the intermediate (G_I) is the dominant whereas, if the G_O - and/or G_R -terms predominate with respect to G_I , it follows that $\Delta E_{app}^{0'} > \Delta E^{0'}$ and an *apparent* potential inversion or cooperative [23, 29] situation may arise.

Fig. 1 shows the cyclic voltammograms at a microdisc electrode of two-electron processes where the oxidized or reduced species take part in chemical equilibria in solution and not the intermediate, which would be highly stable in the absence of chemical effects:

$\Delta E^{0'} = -200 \text{ mV}$. The value of the surface concentrations are also calculated to show the change in the stability of the redox states as a function of the applied potential and of the G_X -value ($X \equiv O, R$). Note that the latter can be modified experimentally by varying the concentration of species L (the larger the c_L^* -value, the larger G_X) and that it takes a null value in the absence of L (Eq. (34)).

In the case of the CEE or the CCEE mechanisms (Figures 1a and 1b), only the oxidized species O is involved in homogeneous chemical equilibria ($G_I = G_R = 0$) that stabilize it such that the depletion of the OL_i species by the electrode reaction takes place at more negative potentials (see Figure 1b) whereas the effect on the surface concentration of the reduced species is negligible (not shown). The stability of the intermediate is also strongly affected. As a result of the homogeneous chemical processes (*i.e.*, as G_O increases), the "life potential range" of the intermediate (defined as the potential range where the surface concentration of the intermediate takes significant values) and its surface concentration are smaller. Moreover, the beginning of the potential region where IL_i are somewhat stable is situated at more negative potentials (see Figure 1b and Section 3.3). These effects give rise to the shift of the first electro-reduction peak, the second one being scarcely affected in such a way that, eventually, they may merge into one in spite of the large difference between the formal potentials ($\Delta E^{0'} = -200 \text{ mV}$).

The "mirror image" situation where it is the reduced species R that undergoes a strong chemical stabilization in solution is considered in Figures 1c and 1d; this would correspond to the EEC or the EECC mechanisms ($G_O = G_I = 0$). The intermediate surface concentration decreases when G_R increases and IL_i "disappear" at less negative potentials. With regard to the voltammetric response, the two signals move closer as c_L^* is increased and they can merge into one. Nevertheless, the change of the c_L^* -value only has a significant effect on the position of the second signal in the EEC(C) mechanisms, which can be easily distinguished from the (C)CEE one depending on which curve shifts as c_L^* is modified.

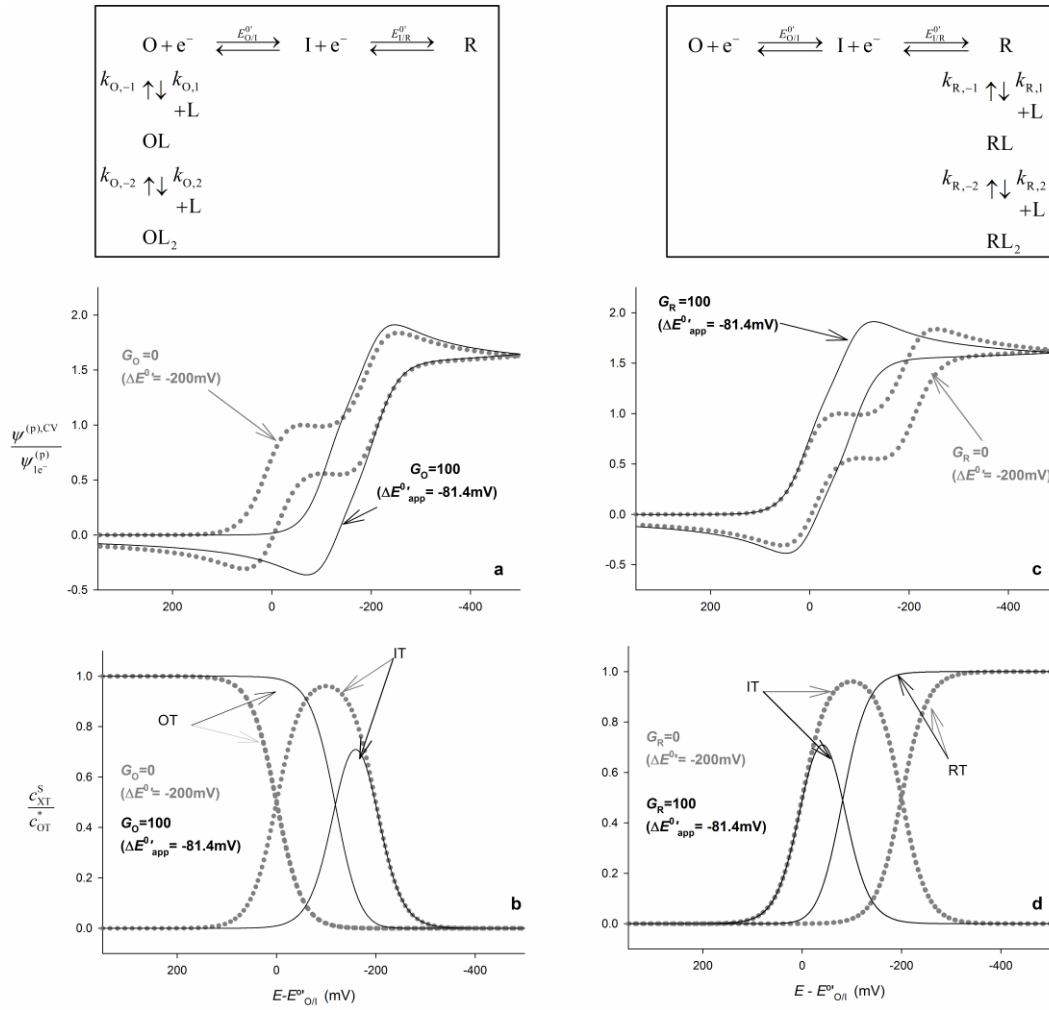


Figure 1. Influence of coupled chemical equilibria involving *only* the oxidized species (**a** and **b**, G_O values indicated on the graphs) or *only* the reduced species (**c** and **d**, G_R indicated on the graphs) for $\Delta E^{0'} = -200$ mV. Cyclic voltammograms (**a** and **c**, Eq. (30)) and normalized surface concentrations (**b** and **d**, Eqs. (16)) at a microdisc electrode ($r_d \approx 30 \mu\text{m}$), $\nu = 100 \text{ mV s}^{-1}$, $D = 10^{-5} \text{ cm}^2 \text{ s}^{-1}$, $|\Delta E| = 0.01 \text{ mV}$, $T = 298 \text{ K}$

When the formal potentials are not very different and a single voltammogram is obtained (Figure 2), the occurrence of the chemical processes can be detected in the change of the position and shape of the voltammogram as c_L^* is varied. For the two types of mechanism considered in Figure 2, an increase of c_L^* leads to larger $\Delta E_{\text{app}}^{0'}$ -values, to larger peak currents and smaller peak-to-peak separations. On the other hand, the shift of the position of the voltammograms with c_L^* enables us to discriminate between the (C)CEE and EEC(C) cases given that it takes place in opposite directions. Also, note that under these conditions (*i.e.*, $\Delta E^{0'} = 0 \text{ mV}$) the "life potential range" of *all* the species is affected by G_O or G_R .

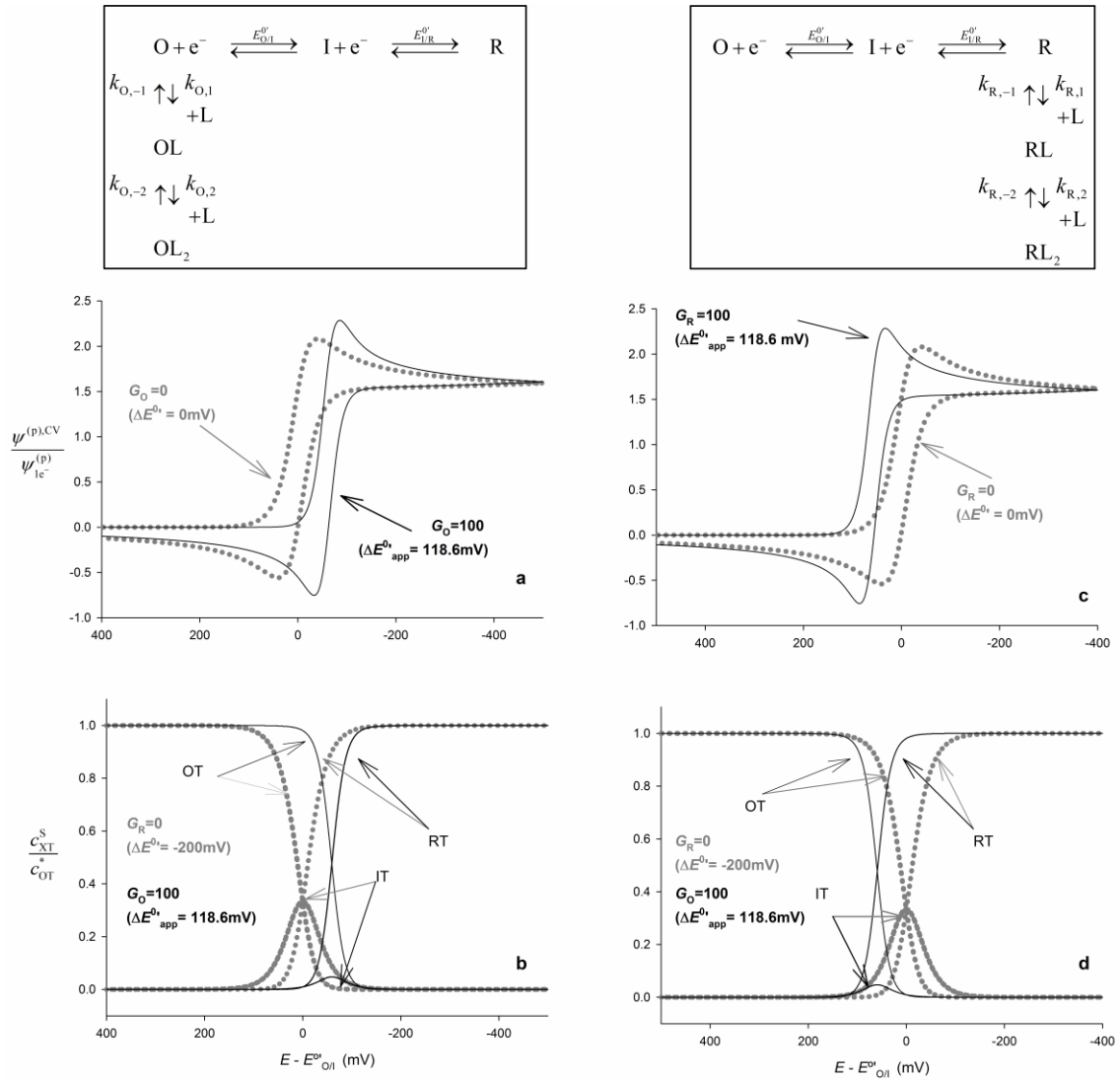


Figure 2. Influence of coupled chemical equilibria involving *only* the oxidized species (**a** and **b**, G_O values indicated on the graphs) or *only* the reduced species (**c** and **d**, G_R indicated on the graphs) for $\Delta E^{0'} = 0$ mV. Cyclic voltammograms (**a** and **c**, Eq. (30)) and normalized surface concentrations (**b** and **d**, Eqs. (16)) at a microdisc electrode ($r_d \approx 30 \mu\text{m}$), $\nu = 100 \text{ mV s}^{-1}$, $D = 10^{-5} \text{ cm}^2 \text{ s}^{-1}$, $|\Delta E| = 0.01 \text{ mV}$, $T = 298 \text{ K}$

The situation where it is only the intermediate species that is involved in homogeneous chemical equilibria ($G_O = G_R = 0$) is studied in Figure 3 for both $\Delta E^{0'} = -200 \text{ mV}$ and 0 mV . In this situation, the increase of c_L^* (and so of G_I) leads to the decrease of $\Delta E_{app}^{0'}$ (Eq. (37)) with the first signal shifting to more positive potentials and the second one towards more negative E -values in a symmetric way with respect to the average apparent formal potential $\bar{E}_{app}^{0'} = \frac{E_{OT/IT}^{0'} + E_{IT/RT}^{0'}}{2}$. As a result, when the c_L^* -value is increased, the CV curve tends to split in two (Figure 3a) and the two peaks separate from each other (Figure 3b).

According to the results shown in Figures 1-3, one can conclude that the increase of the concentration of L has different effects on the voltammograms depending on whether the corresponding chemical equilibria mostly affect the oxidized, reduced or intermediate species. In the latter case, the split of the voltammograms takes place whereas the signals tend to merge into one when the oxidized and/or the reduced states show a more significant chemical stabilization.

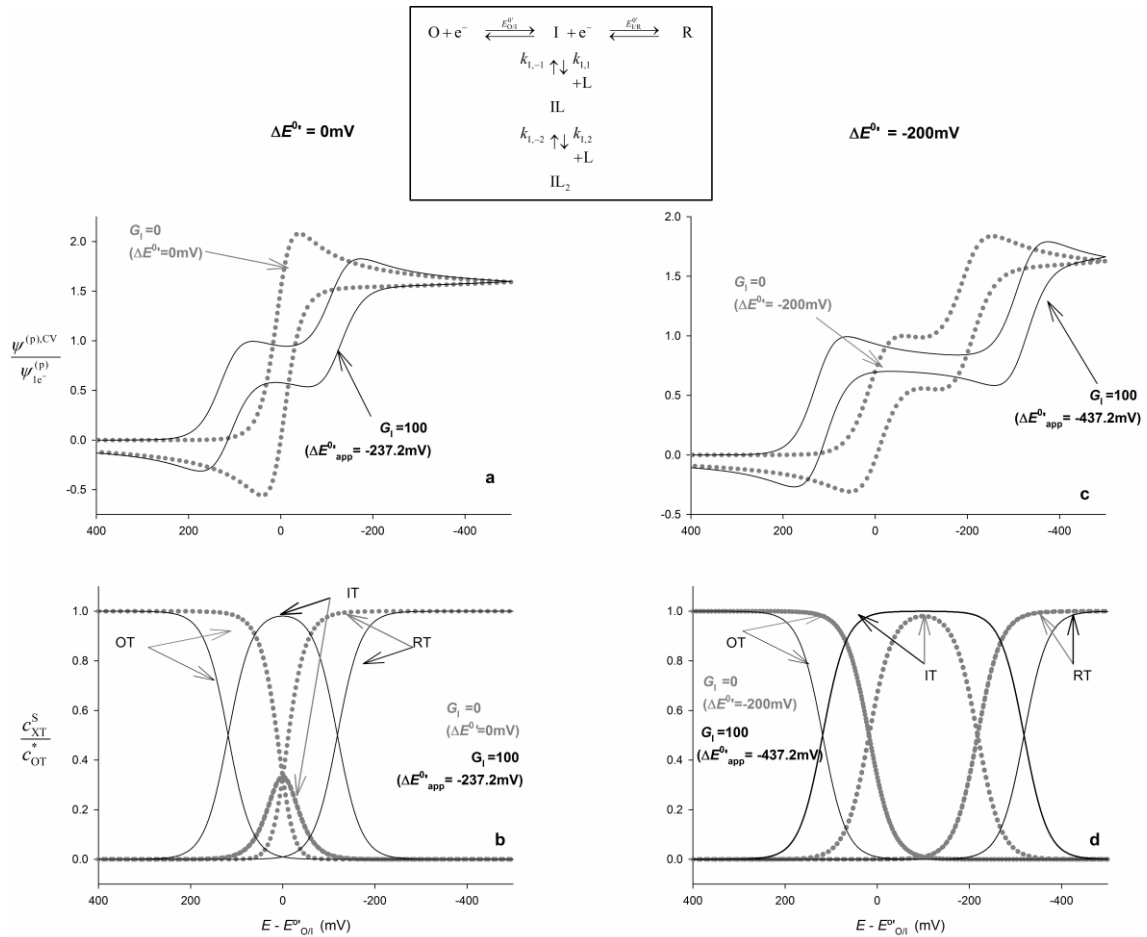


Figure 3. Influence of coupled chemical equilibria involving *only* the intermediate species (G_I values indicated on the graphs) for $\Delta E^{\text{O/I}} = 0$ mV (**a** and **b**) and $\Delta E^{\text{O/I}} = -200$ mV (**c** and **d**). Cyclic voltammograms (**a** and **c**, Eq. (30)) and normalized surface concentrations (**b** and **d**, Eqs. (16)) at a microdisc electrode ($r_d \approx 30$ μm), $\nu = 100$ mV s^{-1} , $D = 10^{-5}$ $\text{cm}^2 \text{s}^{-1}$, $|\Delta E| = 0.01$ mV, $T = 298$ K

3.2. Electrode geometry

Microelectrodes offer very valuable advantages for accurate experimental studies by minimizing non-faradaic and ohmic drop effects [13]. However, the theoretical treatment of the electrochemical response at microelectrodes is, in general, more complicated than for macroelectrodes as a consequence of the non-uniform accessibility to the electrode surface of the electroactive species at some geometries such as at microdiscs. The theory presented in Section 2 enables us to overcome these difficulties and calculate the response in cyclic voltammetry at the most common ones. Thus, Figure 4 shows the CV curves calculated from Eq. (32) at electrodes of very different size (from macroelectrodes to ultramicroelectrodes) and shape (disc, (hemi)spherical, band and cylindrical).

As can be observed, the electrode geometry affects the shape of the voltammograms and the magnitude of the current density, differences being null at macroelectrodes (linear diffusion) and increasingly apparent as the electrode size shrinks. Under transient conditions, a peak shape is obtained whatever the electrode shape with the current density increasing in the order: cylinder < band < (hemi)sphere < disc. At ultramicroelectrodes, a peak-shaped pseudo-stationary response is observed at microcylinders and microbands (see Figures 4e and 4f) [19] in contrast to the sigmoid steady state response attained at microdiscs and micro(hemi)spheres where the "total" limiting current is $2 \times I_D$ independently of the $\Delta E_{app}^{0'}$ -value. For studies with ultramicroelectrodes, the use of a differential technique like D(S)CV is recommended since it offers well-defined, peak-shaped signals that enables easier and more accurate quantitative analysis (see insets in Figures 4e and 4f and Section 3.3). Also note that D(S)CV is particularly useful for any electrode geometry when there is partial overlapping of the CV curves of the two-electron transfers since differential techniques generally provide better resolution of the two signals [31, 34, 35].

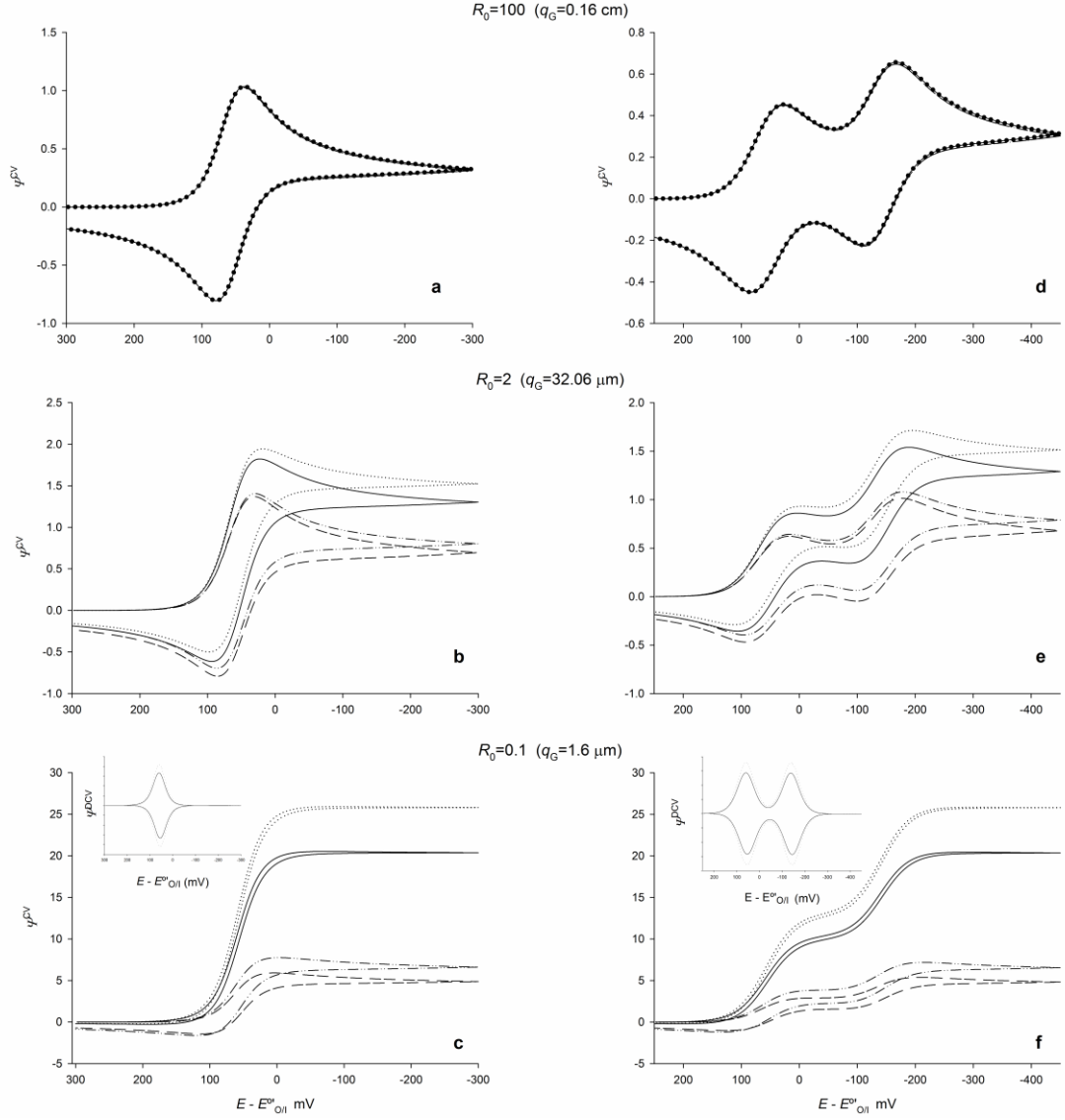


Figure 4. Influence of the electrode size ($R_0 = q_G \sqrt{Fv/(DRT)}$) and shape on the CV response (Eq. (30)) for the most usual geometries: disc (—), spherical (---), band (— · —) and cylindrical (- - -) and for $\Delta E^{0'} = 0$ mV (a-c) and $\Delta E^{0'} = -200$ mV (d-f), $v = 100$ mV s⁻¹, $D = 10^{-5}$ cm² s⁻¹, $|\Delta E| = 0.01$ mV, $T = 298$ K. At ultramicroelectrodes (c and f), the DCV responses for disc and spherical electrodes are also shown as insets: $\Psi^{DCV} = \Psi^{(p+1),CV} - \Psi^{(p),CV}$, $G_0 = 10$, $G_1 = 100$, $G_R = 1000$.

3.3. Determination of the stability constants and formal potentials

The determination of the reaction mechanism and the values of the equilibrium constants and formal potentials can be performed by fitting the variation of the *apparent* formal potentials with the concentration of species L with Eqs. (13). As discussed in Section 3.1, the change of c_L^* will affect in a different way the $\Delta E_{app}^{0'}$ -value and so the shape of the

voltammogram, depending on which species takes part in homogeneous chemical equilibria and the stoichiometry of such process(es).

The value of $\Delta E_{app}^{0'}$ can be determined from the forward peak current ($\Psi_{f,p}$, Figure 5a) and the peak-to-peak separation (ΔE_{peak} , Figure 5b) of the cyclic voltammogram and (then) the individual values of $E_{OT/IT}^{0'}$ and $E_{IT/RT}^{0'}$ can be obtained from the peak potential(s) (Figure 5c). In the region where two signals are observed, the values of $\Psi_{f,p}$, ΔE_{peak} and $E_{f,p}$ in Figure 5 refer to the first one.

Under transient conditions, $\Psi_{f,p}$ increases continuously with $\Delta E_{app}^{0'}$ at both macro- and micro-electrodes from the value corresponding to a one-electron transfer to that of an "apparently simultaneous" two electron transfer. At macroelectrodes the well-known lower and upper limit $\Psi_{f,p}$ -values are 0.446 and 1.26 [14, 15] and empirical equations for microdiscs and micro(hemi)spheres were reported in [35]. With respect to ΔE_{peak} , the variation with $\Delta E_{app}^{0'}$ also depends on the geometry of the electrode in such a way that larger peak-to-peak separations are observed at microelectrodes. Thus, for example, at 298 K the ΔE_{peak} -value ranges between *ca.* 57mV and 28.5mV at macroelectrodes for "independent" and "simultaneous" two-electron transfers respectively [14, 15], whereas ΔE_{peak} varies from *ca.* 160mV to 70 mV at a microdisc of

$$R_0 = q_G \sqrt{\frac{F\nu}{DRT}} = 1 \text{ (with } q_G \text{ being the electrode radius).}$$

The position of the voltammogram(s) enables the determination of $E_{OT/IT}^{0'}$ and $E_{IT/RT}^{0'}$. As was shown in Figure 5c, the enhancement of the diffusive mass transport (*i.e.*, the decrease of the electrode size and the use of discs rather than hemispheres) shifts the peaks to more negative potentials. Thus, for very negative $\Delta E_{app}^{0'}$ -values, the forward peak potential ($E_{f,p}$) of the first peak takes the well known value for one-electron reductions $E_{OT/IT}^{0'} - 28 \text{ mV}$ at macroelectrodes [14, 15] and $E_{f,p} = E_{OT/IT}^{0'} - 81 \text{ mV}$ at a microdisc electrode with $R_0 = 1$. Also, the two CV curves show a centre of symmetry (see Figures 1 and 3) the abscissa value of which

coincides with the average *apparent* formal potential $\bar{E}_{app}^{0'} = \frac{E_{OT/IT}^{0'} + E_{IT/RT}^{0'}}{2}$. For very positive $\Delta E_{app}^{0'}$ -values, the forward peak potential of the single wave is given by $E_{f,p} = \bar{E}_{app}^{0'} - 14$ mV at macroelectrodes and by $E_{f,p} = \bar{E}_{app}^{0'} - 34$ mV at a microdisc with $R_0 = 1$.

For $R_0 < 1$, the system approaches steady state conditions and the peak of the cyclic voltammograms becomes less defined. Eventually, when the steady state response is achieved at microdiscs and micro(hemi)spheres ($R_0 < 0.1$), the use of D(S)CV is more convenient (see Section 3.2) and the difference between the *apparent* formal potentials can be obtained from the peak current and half-peak width (Figures 6a and 6b). The $E_{OT/IT}^{0'}$ and $E_{IT/RT}^{0'}$ -values can be determined from the peak potential(s), which coincides with the apparent formal potential for $\Delta E_{app}^{0'} < -140$ mV and with their average value $\bar{E}_{app}^{0'}$ for $\Delta E_{app}^{0'} > -70$ mV [23]. Note that the shape and position of the D(S)CV signal (that is, the $w_{1/2}$ and ΔE_{peak} values) are independent of the electrode geometry, which is very convenient since the data obtained are not affected by uncertainties related to the electrode size and shape.

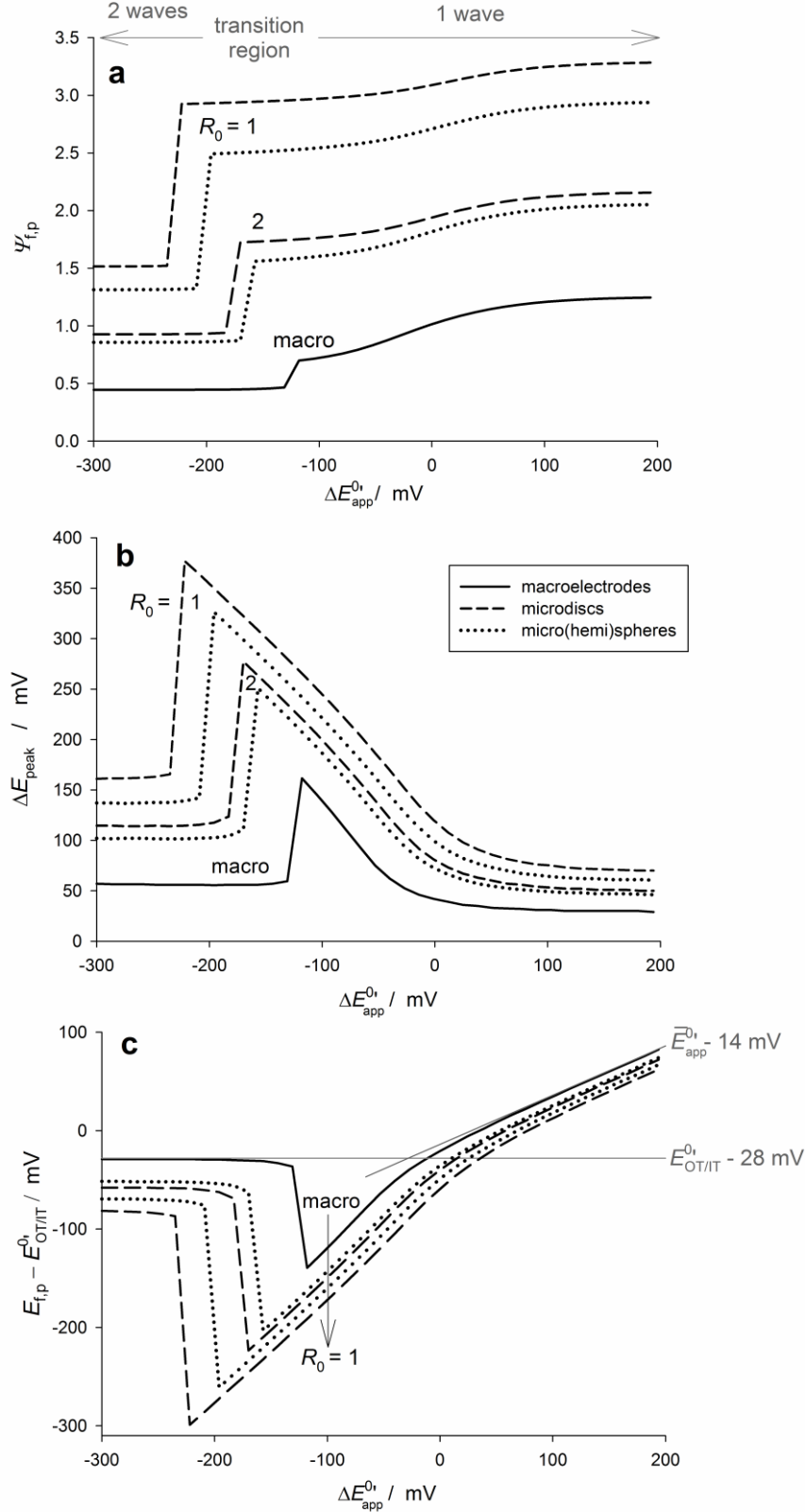


Figure 5. Variation of the dimensionless forward peak current (a), peak-to-peak separation (b) and forward peak potential (c) in cyclic voltammetry with the difference between the *apparent* formal potentials at macroelectrodes (solid line), microdiscs ($R_0 = q_G \sqrt{Fv/(DRT)} = 2$ and 1, dashed line) and micro(hemi)spheres (dotted line). Values obtained from Eq. (30) and corresponding to the first signal in the region where two waves are observed. $T = 298$ K, $E_{vertex} - E_{OT/IT}^{0'} = -600$ mV, $\Delta E = 0.01$ mV

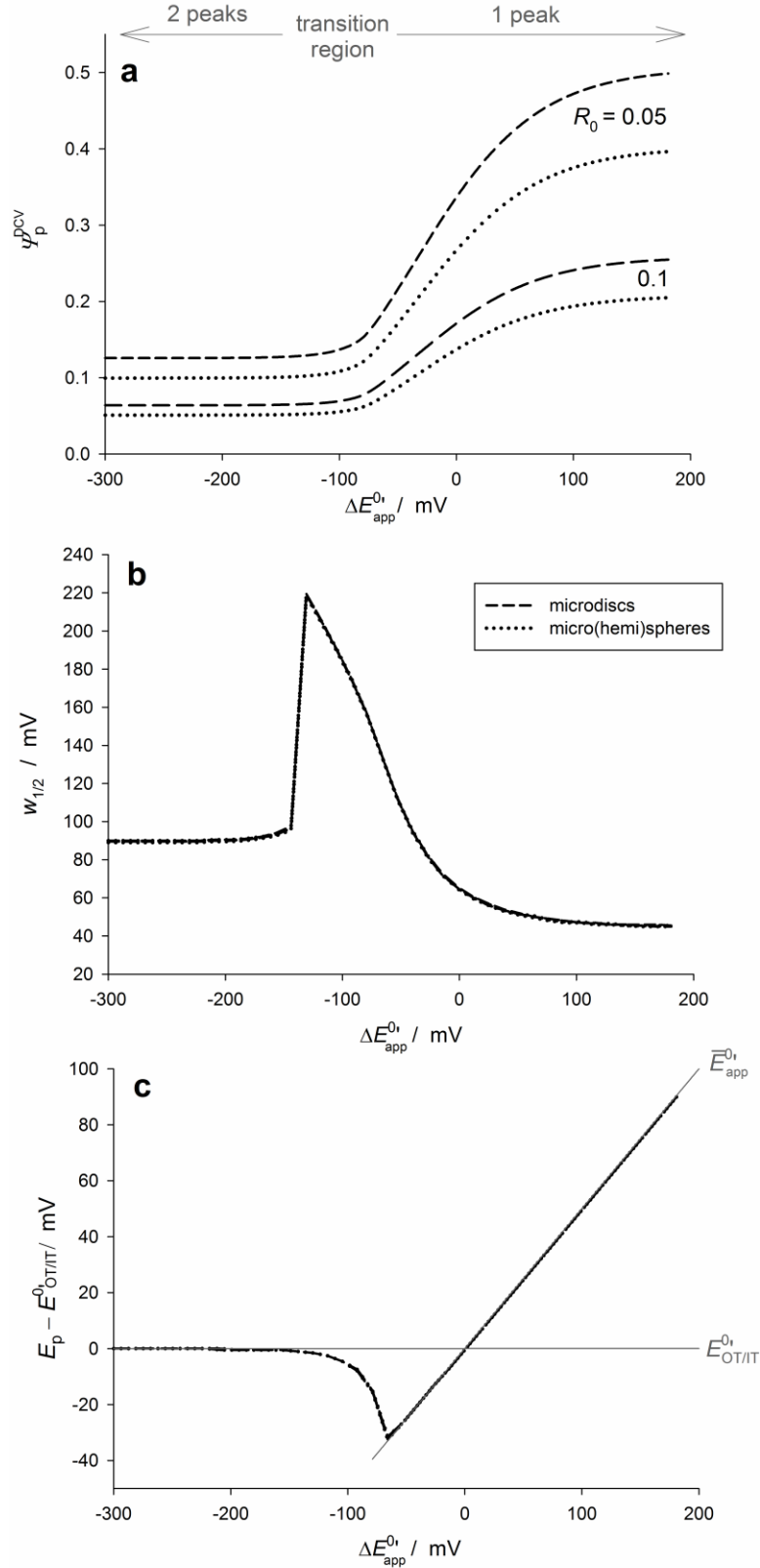


Figure 6. Variation of the dimensionless forward peak current (a), half-peak width (b) and forward peak potential (c) in differential cyclic voltammetry with the difference between the *apparent* formal potentials at microdiscs (dashed line) and micro(hemi)spheres (dotted line) for $R_0 = q_G \sqrt{Fv/(DRT)} = 0.1$ and 0.05. Values obtained from Eq. (30) and corresponding to the first peak in the region where two peaks are observed. Other conditions as in Figure 5.

4. Conclusions

A simple analytical expression has been deduced for the response of the 9-member square scheme in cyclic voltammetry and differential cyclic voltammetry at microdiscs, micro(hemi)spheres, microbands and microcylinders. This has enabled us to investigate the effects of physical (mass transfer) and chemical (coupled homogeneous reactions) phenomena on the voltammetric response.

When the coupled chemical equilibria mainly stabilize the oxidized and/or reduced species, there is an apparent increase of the difference between the formal potentials so that the "life potential range" of the intermediate redox state decreases and the two voltammograms tend to merge into one. The opposite behaviours are observed when the intermediate species is the most stabilized by chemical processes in solution such that the signals tend to split in two.

The determination of the formal potentials and the equilibrium constants can be performed from the variation with the concentration of species L of the values of the two *apparent* formal potentials. In order to obtain the latter, working curves have been given for microdiscs and micro(hemi)spheres under transient conditions based on the peak current, peak potential(s) and peak-to-peak separation of the cyclic voltammograms. The values of all the above magnitudes are dependent on the electrode geometry such that the well-known criteria for macroelectrodes do not apply at microelectrodes. At disc and hemispherical ultramicroelectrodes under steady state conditions, the use of differential cyclic voltammetry is beneficial and the values of the apparent formal potentials can be obtained from the peak current, peak potential(s) and half-peak width. The last two magnitudes are independent of the ultramicroelectrode shape and size and then possible geometry-related uncertainties do not affect the accuracy of the quantitative analysis.

Acknowledgements

The authors greatly appreciate financial support provided by the "Fundación Séneca de la Región de Murcia" (Projects 19887/GERM/15 and 18968/JLI/13) as well as by the "Ministerio de Economía y Competitividad" of the Spanish Government (Projects CTQ-2015-71955-REDT and CTQ-2015-65243-P-Newtwork of Excellence "Sensors and Biosensors"). EL also thanks the "Ministerio de Economía y Competitividad" for the contract "Juan de la Cierva-Incorporación 2015" and JMGG the University of Murcia and Banco Santander for the fellowship under the programme "Contratos Predoctorales FPU 2016".

Appendix. Particular reaction schemes

The analytical solution for single-pulse techniques of the most common particular cases derived from Scheme I are presented in Tables A1 and A2.

Mechanism		Conditions	I-E response	$E_{1/2}$
E	$O + e^- \xrightleftharpoons{E_{O/I}^{0'}} I$	$\left. \begin{array}{l} e^{\eta_{IT/RT}} \rightarrow \infty \\ \beta_{O,v} = \beta_{I,v} = 0 \end{array} \right\}$	$I_N^E = \frac{I^E}{I_D} = \frac{1}{1 + e^{\eta_{O/I}}}$	$E_{1/2}^E = E_{O/I}^{0'}$
EC	$O + e^- \xrightleftharpoons{E_{O/I}^{0'}} I$ $\uparrow\downarrow + L$ IL	$\left. \begin{array}{l} e^{\eta_{IT/RT}} \rightarrow \infty \\ \beta_{I,1} \neq 0 \\ \beta_{O,1} = \beta_{O,2} = \beta_{I,2} = 0 \end{array} \right\}$	$I_N^{EC} = \frac{1 + K_{I,1}}{1 + K_{I,1} + e^{\eta_{O/I}}}$	$E_{1/2}^{EC} = E_{O/I}^{0'} + \frac{RT}{F} \ln[1 + K_{I,1}]$
CE	$O + e^- \xrightleftharpoons{E_{O/I}^{0'}} I$ $\uparrow\downarrow + L$ OL	$\left. \begin{array}{l} e^{\eta_{IT/RT}} \rightarrow \infty \\ \beta_{O,1} \neq 0 \\ \beta_{O,2} = \beta_{I,1} = \beta_{I,2} = 0 \end{array} \right\}$	$I_N^{CE} = \frac{1}{1 + (1 + K_{O,1})e^{\eta_{O/I}}}$	$E_{1/2}^{CE} = E_{O/I}^{0'} - \frac{RT}{F} \ln[1 + K_{O,1}]$
4-member square scheme	$O + e^- \xrightleftharpoons{E_{O/I}^{0'}} I$ $\uparrow\downarrow + L$ OL + $e^- \xrightleftharpoons{E_{OL/IL}^{0'}} IL$	$\left. \begin{array}{l} e^{\eta_{IT/RT}} \rightarrow \infty \\ \beta_{O,1}, \beta_{I,1} \neq 0 \\ \beta_{O,2} = \beta_{I,2} = 0 \end{array} \right\}$	$I_N^{4Sq.} = \frac{1 + K_{I,1}}{1 + K_{I,1} + (1 + K_{O,1})e^{\eta_{O/I}}}$	$E_{1/2}^{4Sq.} = E_{O/I}^{0'} + \frac{RT}{F} \ln \frac{1 + K_{I,1}}{1 + K_{O,1}}$
Ladder scheme	$O + e^- \xrightleftharpoons{E_{O/I}^{0'}} I$ $\uparrow\downarrow + L$ OL + $e^- \xrightleftharpoons{E_{OL/IL}^{0'}} IL$ $\uparrow\downarrow + L$ OL ₂ + $e^- \xrightleftharpoons{E_{OL_2/IL_2}^{0'}} IL_2$	$\left. \begin{array}{l} e^{\eta_{IT/RT}} \rightarrow \infty \\ \beta_{O,v}, \beta_{I,v} \neq 0 \end{array} \right\}$	$I_N^{Q-Fe} = \frac{1 + K_{I,1} + \beta_{I,2}}{1 + K_{I,1} + \beta_{I,2} + (1 + K_{O,1} + \beta_{O,2})e^{\eta_{O/I}}}$	$E_{1/2}^{Q-Fe} = E_{O/I}^{0'} + \frac{RT}{F} \ln \frac{1 + K_{I,1} + \beta_{I,2}}{1 + K_{O,1} + \beta_{I,2}}$

Table A1. Particular cases derived from the 9-member square mechanism where an (apparent) one-electron transfer takes place.

Mechanism		Conditions	I-E response ^b	$E_{1/2}$ ^{a,b}
EE	$\text{O} + \text{e}^- \xrightleftharpoons{E_{\text{O/I}}^{0'}} \text{I} + \text{e}^- \xrightleftharpoons{E_{\text{I/R}}^{0'}} \text{R}$	$\beta_{\text{O,v}} = \beta_{\text{I,v}} = 0$	$I_{\text{N}}^{\text{EE}} = \frac{I^{\text{EE}}}{I_{\text{D}}} = \frac{2 + e^{\eta_{\text{I/R}}}}{1 + e^{\eta_{\text{I/R}}} (1 + e^{\eta_{\text{O/I}}})}$ $\text{b} \begin{cases} I_{\text{N}}^{\text{EE},1\text{st}} = \frac{1}{1 + e^{\eta_{\text{O/I}}}} \\ I_{\text{N}}^{\text{EE},2\text{nd}} = \frac{1}{1 + e^{\eta_{\text{I/R}}}} \end{cases}$	$\text{a} E_{1/2}^{\text{EE}} = \frac{E_{\text{O/I}}^{0'} + E_{\text{I/R}}^{0'}}{2}$ $\text{b} \begin{cases} E_{1/2}^{\text{EE},1\text{st}} = E_{\text{O/I}}^{0'} \\ E_{1/2}^{\text{EE},1\text{st}} = E_{\text{I/R}}^{0'} \end{cases}$
ECE	$\begin{array}{c} \text{O} + \text{e}^- \xrightleftharpoons{E_{\text{O/I}}^{0'}} \text{I} \\ \uparrow \downarrow + \text{L} \\ \text{IL} + \text{e}^- \xrightleftharpoons{E_{\text{IL/RL}}^{0'}} \text{RL} \end{array}$	$\left. \begin{array}{l} \beta_{\text{O},1} = \beta_{\text{O},2} = 0 \\ \beta_{\text{I},1} \neq 0; \beta_{\text{I},2} = 0 \end{array} \right\}$	$I_{\text{N}}^{\text{ECE}} = \frac{2 + (1 + K_{\text{I},1})e^{\eta_{\text{I/R}}}}{1 + (1 + K_{\text{I},1})e^{\eta_{\text{I/R}}} (1 + e^{\eta_{\text{O/I}}})}$ $\text{b} \begin{cases} I_{\text{N}}^{\text{ECE},1\text{st}} = \frac{1 + K_{\text{I},1}}{1 + K_{\text{I},1} + e^{\eta_{\text{O/I}}}} \\ I_{\text{N}}^{\text{ECE},2\text{nd}} = \frac{1}{1 + (1 + K_{\text{I},1})e^{\eta_{\text{I/R}}}} \end{cases}$	$\text{a} E_{1/2}^{\text{ECE}} = \frac{E_{\text{O/I}}^{0'} + E_{\text{I/R}}^{0'}}{2}$ $\text{b} \begin{cases} E_{1/2}^{\text{ECE},1\text{st}} = E_{\text{O/I}}^{0'} + \frac{RT}{F} \ln(1 + K_{\text{I},1}) \\ E_{1/2}^{\text{ECE},1\text{st}} = E_{\text{I/R}}^{0'} - \frac{RT}{F} \ln(1 + K_{\text{I},1}) \end{cases}$
EQ-Fence	$\begin{array}{ccccc} \text{O} + \text{e}^- & \xrightleftharpoons{E_{\text{O/I}}^{0'}} & \text{I} + \text{e}^- & \xrightleftharpoons{E_{\text{I/R}}^{0'}} & \text{R} \\ \uparrow \downarrow + \text{L} & & \uparrow \downarrow + \text{L} & & \uparrow \downarrow + \text{L} \\ \text{OL} + \text{e}^- & \xrightleftharpoons{E_{\text{OL/IL}}^{0'}} & \text{IL} + \text{e}^- & \xrightleftharpoons{E_{\text{IL/RL}}^{0'}} & \text{RL} \end{array}$	$\left. \begin{array}{l} \beta_{\text{O},1} \neq 0; \beta_{\text{I},1} \neq 0; \beta_{\text{R},1} \neq 0 \\ \beta_{\text{O},2} = \beta_{\text{I},2} = \beta_{\text{R},2} = 0 \end{array} \right\}$	$I_{\text{N}}^{\text{EQ-Fe}} = \frac{2(1 + K_{\text{R},1}) + (1 + K_{\text{I},1})e^{\eta_{\text{I/R}}}}{(1 + K_{\text{R},1}) + (1 + K_{\text{I},1})e^{\eta_{\text{I/R}}} + (1 + K_{\text{O},1})e^{\eta_{\text{O/I}}}e^{\eta_{\text{I/R}}}}$ $\text{b} \begin{cases} I_{\text{N}}^{\text{EQ},1\text{st}} = \frac{1 + K_{\text{I},1}}{(1 + K_{\text{I},1}) + (1 + K_{\text{O},1})e^{\eta_{\text{O/I}}}} \\ I_{\text{N}}^{\text{EQ},2\text{nd}} = \frac{1 + K_{\text{R},1}}{(1 + K_{\text{R},1}) + (1 + K_{\text{I},1})e^{\eta_{\text{I/R}}}} \end{cases}$	$\text{a} E_{1/2}^{\text{EQ}} = \frac{1}{2} \left[(E_{\text{O/I}}^{0'} + E_{\text{I/R}}^{0'}) - \frac{RT}{F} \ln \left(\frac{1 + \beta_{\text{O},1}}{1 + \beta_{\text{R},1}} \right) \right]$ $\text{b} \begin{cases} E_{1/2}^{\text{EQ},1\text{st}} = E_{\text{O/I}}^{0'} - \frac{RT}{F} \ln \left(\frac{1 + \beta_{\text{O},1}}{1 + \beta_{\text{I},1}} \right) \\ E_{1/2}^{\text{EQ},1\text{st}} = E_{\text{I/R}}^{0'} - \frac{RT}{F} \ln \left(\frac{1 + \beta_{\text{I},1}}{1 + \beta_{\text{R},1}} \right) \end{cases}$
9-member square scheme	Scheme I	$\left. \begin{array}{l} \beta_{\text{O},1}, \beta_{\text{O},2} \neq 0 \\ \beta_{\text{I},1}, \beta_{\text{I},2} \neq 0 \\ \beta_{\text{R},1}, \beta_{\text{R},2} \neq 0 \end{array} \right\}$	$I_{\text{N}}^{9\text{Sq.}} = \frac{I^{9\text{Sq.}}}{I_{\text{D}}} = \frac{2(1 + \beta_{\text{R},1} + \beta_{\text{R},2}) + (1 + \beta_{\text{I},1} + \beta_{\text{I},2})e^{\eta_{\text{I/R}}}}{(1 + \beta_{\text{R},1} + \beta_{\text{R},2}) + e^{\eta_{\text{I/R}}} (1 + \beta_{\text{I},1} + \beta_{\text{I},2}) + e^{\eta_{\text{I/R}}} e^{\eta_{\text{O/I}}} (1 + \beta_{\text{O},1} + \beta_{\text{O},2})}$ $\text{b} \begin{cases} I_{\text{N}}^{9\text{Sq.},1\text{st}} = \frac{1 + \beta_{\text{I},1} + \beta_{\text{I},2}}{(1 + \beta_{\text{I},1} + \beta_{\text{I},2}) + (1 + \beta_{\text{O},1} + \beta_{\text{O},2})e^{\eta_{\text{O/I}}}} \\ I_{\text{N}}^{9\text{Sq.},2\text{nd}} = \frac{1 + \beta_{\text{R},1} + \beta_{\text{R},2}}{(1 + \beta_{\text{R},1} + \beta_{\text{R},2}) + (1 + \beta_{\text{I},1} + \beta_{\text{I},2})e^{\eta_{\text{I/R}}}} \end{cases}$	$\text{a} E_{1/2}^{9\text{Sq.}} = \frac{1}{2} \left[(E_{\text{O/I}}^{0'} + E_{\text{I/R}}^{0'}) - \frac{RT}{F} \ln \left(\frac{1 + \beta_{\text{O},1} + \beta_{\text{O},2}}{1 + \beta_{\text{R},1} + \beta_{\text{R},2}} \right) \right]$ $\text{b} \begin{cases} E_{1/2}^{9\text{Sq.},1\text{st}} = E_{\text{O/I}}^{0'} - \frac{RT}{F} \ln \left(\frac{1 + \beta_{\text{O},1} + \beta_{\text{O},2}}{1 + \beta_{\text{I},1} + \beta_{\text{I},2}} \right) \\ E_{1/2}^{9\text{Sq.},2\text{st}} = E_{\text{I/R}}^{0'} - \frac{RT}{F} \ln \left(\frac{1 + \beta_{\text{I},1} + \beta_{\text{I},2}}{1 + \beta_{\text{R},1} + \beta_{\text{R},2}} \right) \end{cases}$

Table A2. Particular cases derived from the 9-member square mechanism where an (apparent) two-electron transfer takes place. ^a Solutions valid when a single signal is obtained (see Section 3.3). ^b Solutions valid when two well-separated signals are obtained (see Section 3.3).

References

1. Komorsky-Lovrić Š, Lovrić M (2012) Theory of square-wave voltammetry of two electron reduction with the intermediate that is stabilized by complexation. *Electrochim Acta* 69:60–64.
2. Lin Q, Li Q, Batchelor-Mcauley C, Compton RG (2015) Two-electron, Two-proton oxidation of catechol: Kinetics and apparent catalysis. *J Phys Chem C* 119:1489–1495.
3. Batchelor-McAuley C, Li Q, Dapin SM, Compton RG (2010) Voltammetric characterization of DNA intercalators across the full pH range: Anthraquinone-2,6-disulfonate and anthraquinone-2-sulfonate. *J Phys Chem B* 114:4094–4100.
4. Geiger WE, Barrière F (2010) Organometallic electrochemistry based on electrolytes containing weakly-coordinating fluoroarylborate anions. *Acc Chem Res* 43:1030–1039.
5. Li Q, Batchelor-McAuley C, Lawrence NS, et al (2011) Electrolyte tuning of electrode potentials: the one electron vs. two electron reduction of anthraquinone-2-sulfonate in aqueous media. *Chem Commun* 47:11426–11428.
6. Batchelor-Mcauley C, Compton RG (2012) Voltammetry of multi-electron electrode processes of organic species. *J Electroanal Chem* 669:73–81.
7. Fischer J, Dejmkova H, Barek J (2011) Electrochemistry of Pesticides and its Analytical Applications. *Curr Org Chem* 15:2923–2935.
8. Oliveira SCB, Oliveira-Brett AM (2010) Boron doped diamond electrode pre-treatments effect on the electrochemical oxidation of dsDNA, DNA bases, nucleotides, homopolynucleotides and biomarker 8-oxoguanine. *J Electroanal Chem* 648:60–66.
9. Bruns D (2004) Detection of transmitter release with carbon fiber electrodes. *Methods* 33:312–321.
10. Sardar R, Funston AM, Mulvaney P, Murray RW (2009) Gold nanoparticles: Past, present, and future. *Langmuir* 25:13840–13851.
11. Jacq J (1971) Schema carre. *J Electroanal Chem Interfacial Electrochem* 29:149–180.
12. Laviron E, Meunier-Prest R (1992) Electrochemical reactions with protonations at equilibrium. *J Electroanal Chem* 324:1–18.
13. Montenegro MI, Queirós MA, Daschbach JL (1991) Microelectrodes: Theory and Applications. Springer Netherlands, Dordrecht
14. Bard AJ, Faulkner LR (2000) *Electrochemical Methods: Fundamentals and Applications*, 2nd ed. Wiley, New York
15. Compton RG, Banks CE (2010) *Understanding Voltammetry*, 2nd ed. Imperial College Press, London
16. López-Tenés M, Serna C, Moreno MM, Molina A (2007) Study of Molecules with Multiple Redox Centers Using Differential Staircase Voltammetry at Spherical Electrodes and Microelectrodes. *Port Electrochim Acta* 25:103–118.
17. Martínez-Ortiz F, Molina A, Laborda E (2011) Electrochemical digital simulation with highly expanding grid four point discretization: Can Crank-Nicolson uncouple diffusion and homogeneous chemical reactions? *Electrochim Acta* 56:5707–5716.
18. Molina A, Gonzalez J, Henstridge MC, Compton RG (2011) Voltammetry of electrochemically reversible systems at electrodes of any geometry: A general, explicit analytical characterization. *J Phys Chem C* 115:4054–4062.

19. Molina A, González J (2016) Pulse Voltammetry in Physical Electrochemistry and Electroanalysis. Springer International Publishing, Berlin
20. Amatore C, Klymenko O, Svir I (2010) A new strategy for simulation of electrochemical mechanisms involving acute reaction fronts in solution: Principle. *Electrochem commun* 12:1170–1173.
21. Evans DH (1990) Solution electron-transfer reactions in organic and organometallic electrochemistry. *Chem Rev* 90:739–751.
22. Molina A, Gonzalez J, Henstridge MC, Compton RG (2011) Analytical expressions for transient diffusion layer thicknesses at non uniformly accessible electrodes. *Electrochim Acta* 56:4589–4594.
23. Lopez-Tenes M, Gonzalez J, Molina A (2014) Two-electron transfer reactions in electrochemistry for solution-soluble and surface-confined molecules: A common approach. *J Phys Chem C* 118:12312–12324.
24. Moreno MM, Molina Á (2005) Further Applications of Cyclic Voltammetry with Spherical Electrodes. *Collect Czechoslov Chem Commun* 70:133–153.
25. Ruić I (1974) On the theory of stepwise electrode processes. *J Electroanal Chem Interfacial Electrochem* 52:331–354.
26. Lovrić M (1979) The three-electron polarographic wave planar diffusion case. *J Electroanal Chem Interfacial Electrochem* 102:143–153.
27. Komorsky Š, Lovrić M (1980) Simple EEE mechanism at DME. *J Electroanal Chem Interfacial Electrochem* 112:169–174.
28. Molina Á, Serna C, López-Tenés M, Moreno MM (2005) Theoretical background for the behavior of molecules containing multiple interacting or noninteracting redox centers in any multipotential step technique and cyclic voltammetry. *J Electroanal Chem* 576:9–19.
29. Evans DH (2008) One-electron and two-electron transfers in electrochemistry and homogeneous solution reactions. *Chem Rev* 108:2113–2144.
30. Batchelor-Mcauley C, Kätelhön E, Barnes EO, et al (2015) Recent Advances in Voltammetry. *ChemistryOpen* 4:224–260.
31. Komorsky-Lovrić S, Lovrić M (2014) Square-wave Voltammetry of Two-step Electrode Reaction. *Int J Electrochem Sci* 9:435–444.
32. Lovrić M, Komorsky-Lovrić Š (2012) Theory of Square-wave Voltammetry of Kinetically Controlled Two-step Electrode Reactions. *Croat Chem Acta* 85:569–575.
33. Komorsky-Lovrić Š, Lovrić M (2007) Electrode Reaction of Adriamycin Interpreted as Two Consecutive Electron Transfers with Stabilization of the Intermediate. *Collect Czechoslov Chem Commun* 72:1398–1406.
34. Mirceski V, Komorsky-Lovric S, Lovric M (2007) Square-Wave Voltammetry: Theory and Application, 2nd ed. Springer, Berlin
35. Molina A, Serna C, Li Q, et al (2012) Analytical Solutions for the Study of Multielectron Transfer Processes by Staircase, Cyclic, and Differential Voltammetries at Disc Microelectrodes. *J Phys Chem C* 116:11470–11479.